03,13

Investigation of the interlayer surface of p-$Bi_{2-x}Sb_xTe_3$ films of topological thermoelectrics by scanning tunneling spectroscopy and microscopy

© L.N. Lukyanova, I.V. Makarenko, O.A. Usov, V.A. Danilov

Ioffe Institute,
St. Petersburg, Russia

E-mail: lidia.lukyanova@mail.ioffe.ru

Received April 11, 2024
Revised May 12, 2024
Accepted June 17, 2024

The morphology of the interlayer van der Waals surface (0001) has been investigated by scanning tunneling microscopy in layered films of topological insulators p-$Bi_{0.5}Sb_{1.5}Te_3$ and p-Bi_2Te_3 prepared by discrete evaporation. A systematization of the impurity and intrinsic defects arising in the film formation process were fulfilled. It is found that in the film of p-$Bi_{0.5}Sb_{1.5}Te_3$ solid solution with low thermal conductivity, the density of tellurium vacancies V_{Te} and the height distortions in the distribution of Te (1) atoms on the (0001) surface increase compared to p-Bi_2Te_3. Local characteristics of the surface electronic states of the Dirac fermions were determined by scanning tunneling spectroscopy. The Dirac point E_D shifts to the top of the valence band in the p-$Bi_{0.5}Sb_{1.5}Te_3$ film with high thermoelectric figure of merit. Despite the fact that the bulk films under investigation exhibit p-type conductivity, electrons are found on the surface of the films, as the Fermi level E_F is located above the Dirac point E_D. Fluctuations of the Dirac point energy $\Delta E_D/\langle E_D\rangle$, the valence band edge $\Delta E_V/\langle E_V\rangle$, and the energy of the surface defect levels E_p in p-$Bi_{0.5}Sb_{1.5}Te_3$ films are reduced compared to p-Bi_2Te_3 films due to the variation of the density of states on the (0001) surface. The obtained values of the energy gap E_g in the studied films is higher than estimated by optical data due to the inversion the edges of the valence and conduction bands in topological insulators.

Keywords: bismuth and antimony chalcogenides, layered films, surface defects, surface fermion concentration, topological insulator.

DOI: 10.61011/PSS.2024.08.59047.86

1. Introduction

Highly efficient thermoelectric materials based on bismuth and antimony chalcogenides [1] may also serve as strong three-dimensional topological insulators (3D TI) with abnormal properties of surface states of Dirac fermions [2–5]. The emergence of topological surface states is associated with electron band inversion and is governed by the strong spin-orbit interaction [2,3]. The bulk of the thermoelectric material is insulating, while surface electrons acquire characteristic metallic properties due to tight coupling between spin and momentum [4,5].

However, topological thermoelectric materials feature a residual bulk conductivity associated with bulk defects [6,7]. Varying the thermoelectric composition, one may achieve a partial reduction of bulk conductivity by compensating the contributions of acceptor and donor intrinsic defects [8,9].

Scanning tunneling microscopy (STM) and scanning tunneling spectroscopy (STS) [10–12] are used to investigate and systematize impurity and intrinsic defects. These methods allow one to retrieve data on the local parameters of surface electronic states of Dirac fermions by analyzing the imaged morphology and differential tunneling conductance spectra dI_t/dU.

The dI_t/dU spectra, which are proportional to the electronic density of states [13], provide an opportunity to determine Dirac point energy E_D and its fluctuations ΔE_D relative to the average value, the positions of edges of the valence band (E_V) and the conduction band (E_C), Fermi level position E_F, energy gap E_g, defect level energy E_P, and surface concentration of fermions n_s. The present study is focused on the morphology and dI_t/dU spectra of layered films of p-Bi_2Te_3 and solid solution p-$Bi_{0.5}Sb_{1.5}Te_3$, which features a high thermoelectric efficiency [14].

2. Morphology

The studied p-Bi_2Te_3 and p-$Bi_{0.5}Sb_{1.5}Te_3$ films with the tetradymite structure consist of anisotropic (−Te(1)−Bi−Te(2)−Bi−Te(1)−) quintets where Bi atoms substitute Sb atoms. The difference between strong covalent chemical bonding with a small addition of ionic bonding between layers in quintets and weak van der Waals forces acting between the quintets is the reason why crystals cleave easily along the Te(1)−Te(1) boundaries in planes (0001). Interlayer surface (0001) perpendicular to crystallographic axis c has the minimum value of free energy in the examined materials. The nuclei of bismuth and antimony

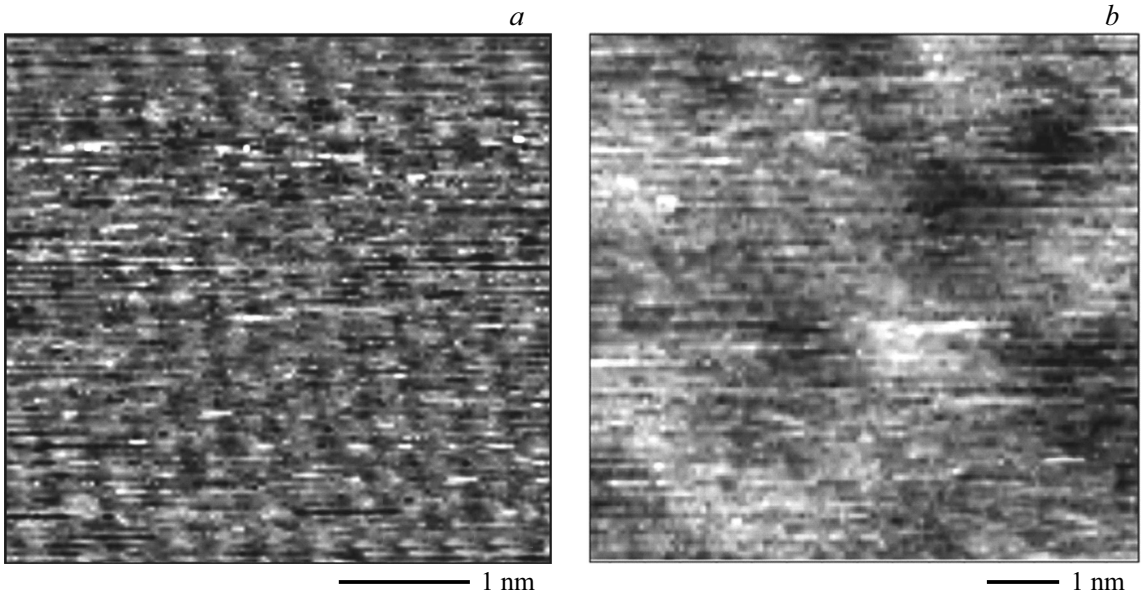

Figure 1. Morphology of surface (0001) in (*a*) *p*-Bi_2Te_3 and (*b*) *p*-$Bi_{0.5}Sb_{1.5}Te_3$. Measurements were carried out (*a*) at tunneling current $I_t = 0.2$ nA and voltage $U = 800$ mV; (*b*) at $I_t = 0.3$ nA and $U = 250$ mV.

chalcogenides are arranged in this case primarily along the *c* axis perpendicular to the substrate plane [15].

Films of *p*-Bi_2Te_3 and solid solution *p*-$Bi_{0.5}Sb_{1.5}Te_3$ for STM/STS studies were obtained by discrete evaporation in an isothermal chamber that provided a vacuum level of $1 \cdot 10^{-6}$ Torr and a homogeneous temperature distribution in the substrate plane. Polyimide tapes up to 20 μm in thickness were used as substrates [14]. The initial thermoelectric material in the form of a powder with grain sizes close to 10 μm was fed into a quartz crucible heated to 800–850 °C, where it evaporated almost instantly and was deposited onto a substrate heated to 250 °C. Excess tellurium was used during the synthesis of *p*-Bi_2Te_3 and *p*-$Bi_{0.5}Sb_{1.5}Te_3$ films to maintain the stoichiometric composition, since Te is a highly volatile component. Thickness t of the obtained films ranged from 0.5 to 3 μm. The films with $t \approx 2\,\mu$m were examined in the present study.

The surface morphology of (0001) films of *p*-Bi_2Te_3 and solid solution *p*-$Bi_{0.5}Sb_{1.5}Te_3$ was studied by STM at a pressure of $1.5 \cdot 10^{-7}$ Pa with a resolution of 0.05 Å at room temperature, direct current, and with feedback enabled (Figure 1). The investigated films had submicrometer thickness. To clean the surface, the top layer of films was peeled off in the high-vacuum chamber with adhesive tape using two mutually perpendicular guides.

The (0001) surface morphology in Bi_2Te_3-based materials is a hexagonal close-packed crystal structure in the *abc* sequence of layers that defines a periodic shift of each layer in quintet (–Te(1)–Bi–Te(2)–Bi–Te(1)–) with respect to the next one [3,16].

Impurity and intrinsic defects in the *p*-$Bi_{0.5}Sb_{1.5}Te_3$ films distort electronic states at fluctuations of the Coulomb potential [16] and affect the intensity of surface morphology images in Figure 1. The distortions of electronic states were attributed in [17,18] to the interaction between layers in the quintets, which results in displacement of atoms in layers and induces curvature of the interlayer van der Waals surface.

Average H_M and root-mean-square H_S height deviations of distortions in the distribution of Te(1) atoms on the surface were determined by analyzing the histograms of the (0001) surface relief plotted based on the morphology images for the *p*-Bi_2Te_3 and *p*-$Bi_{0.5}Sb_{1.5}Te$ films (Figure 1). The average values of $\langle H_M \rangle = 0.068$ nm and $\langle H_S \rangle = 0.033$ nm for the *p*-Bi_2Te_3 films were calculated based on the (0001) surface morphology images. In films *p*-$Bi_{0.5}Sb_{1.5}Te_3$, the values of $\langle H_M \rangle$ and $\langle H_S \rangle$ increase to 0.077 nm and 0.060 nm; i. e., $\langle H_M \rangle$ and $\langle H_S \rangle$ are 13% and 84% larger than the corresponding parameters in the *p*-Bi_2Te_3 films. The growth of $\langle H_M \rangle$ and $\langle H_S \rangle$ in *p*-$Bi_{0.5}Sb_{1.5}Te_3$ solid solution films is attributable to the formation of structural defects and distortion of surface electronic states due to Sb → Bi atomic substitutions [19,20].

Long-wave modulation, which is governed by local distortions of the density of surface electronic states, is seen in the profiles (Figures 2, 3) derived from the (0001) surface morphology (Figure 1). A more pronounced long-wave modulation is found in the *p*-$Bi_{0.5}Sb_{1.5}Te_3$ films with Sb → Bi atomic substitutions. Intensity fluctuations in the form of dark and light spots were observed in the surface morphology of the *p*-$Bi_{0.5}Sb_{1.5}Te_3$ solid solution films (Figure 1), and the values of H_M and H_S increased compared to the *p*-Bi_2Te_3 films.

Surface defects in the investigated *p*-type films manifest themselves as changes in the height distribution between neighboring atoms in surface profiles (Figures 2, 3) and

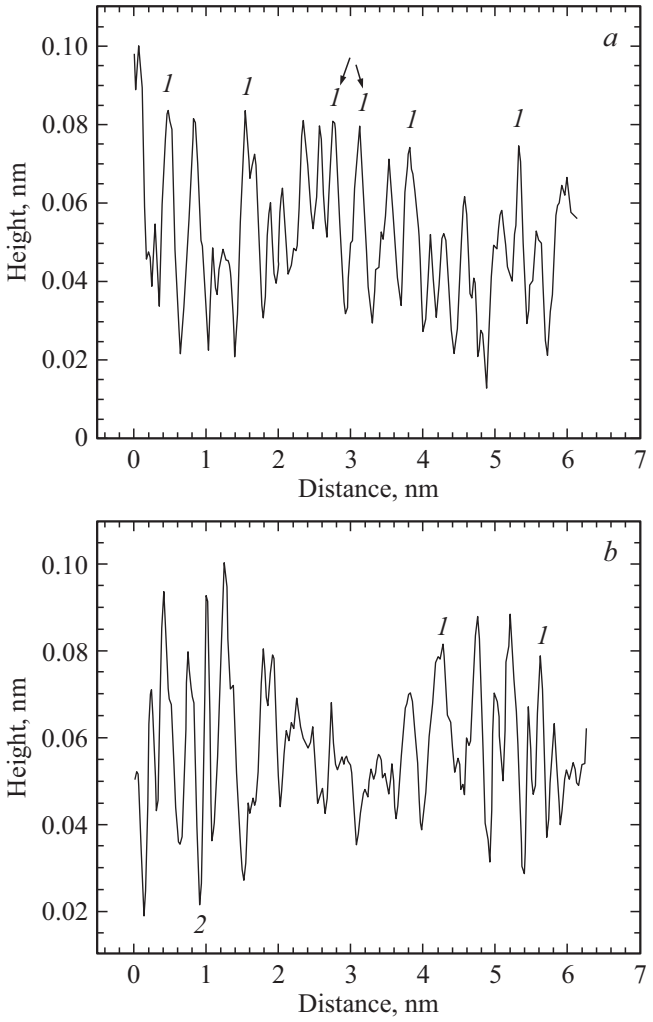

Figure 2. Local (0001) surface profiles of the p-Bi_2Te_3 TI films in different regions of surface morphology images. *1* — Antisite Bi_{Te} defects; arrows indicate closely spaced Bi_{Te} defects. *2* — Te (V_{Te}) vacancy.

shape the (0001) surface relief. The formation of acceptor antisite bismuth Bi_{Te} defects, charged tellurium vacancies V_{Te}, and neutral impurity $Sb \rightarrow Bi$ substitution defects in p-$Bi_{0.5}Sb_{1.5}Te_3$ solid solution films is the most probable in the p-Bi_2Te_3 and p-$Bi_{0.5}Sb_{1.5}Te_3$ films.

In accordance with the difference in diameters of Bi, Sb, and Te atoms, antisite Bi_{Te} defects are manifested in profiles in the form of ~ 0.04 nm peaks, and neutral impurity substitution defects take the form of dips $\sim 0.05-0.06$ nm in depth; the depth of vacancy dips reaches $0.08-0.09$ nm [21,22]. Eight profiles were analyzed for each of the p-Bi_2Te_3 and p-$Bi_{0.5}Sb_{1.5}Te_3$ films to identify defects. The data on surface point defects in the studied films were close to the calculated values obtained in [21]. Aside from the defects marked on surface profiles, the dips and peaks in Figures 2 and 3 may correspond to defects located in the deep layers of the $(-Te(1)-Bi-Te(2)-Bi-Te(1)-)$ quintet.

Acceptor antisite Bi_{Te} defects and tellurium vacancies V_{Te} were found both in the p-Bi_2Te_3 and in the p-$Bi_{0.5}Sb_{1.5}Te_3$ films. However, the V_{Te} vacancy density in the solid solution was higher (Figures 2, 3), which is one of the reasons for the increase in H_M and H_S. The effect of tellurium vacancies V_{Te} on distortions of surface electronic states is likely to be dominant (owing to deeper dips in the (0001) surface profiles and higher formation energy) over the one of neutral $Sb \rightarrow Bi$ substitution defects. Antisite Bi_{Te} defects, which have a lower formation energy than vacancies V_{Te}, have a weaker effect on the values of $\langle H_M \rangle$ and $\langle H_S \rangle$.

In addition, closely spaced pairs of antisite Bi_{Te} defects, which have a stronger effect on thermoelectric properties than individual Bi_{Te} defects, were found in some of the examined profiles [23]. The high density of defects in the p-$Bi_{0.5}Sb_{1.5}Te_3$ solid solution films leads to a significant reduction in thermal conductivity at temperatures below the Debye one ($T_D = 145$ K), but the electrical conductivity also

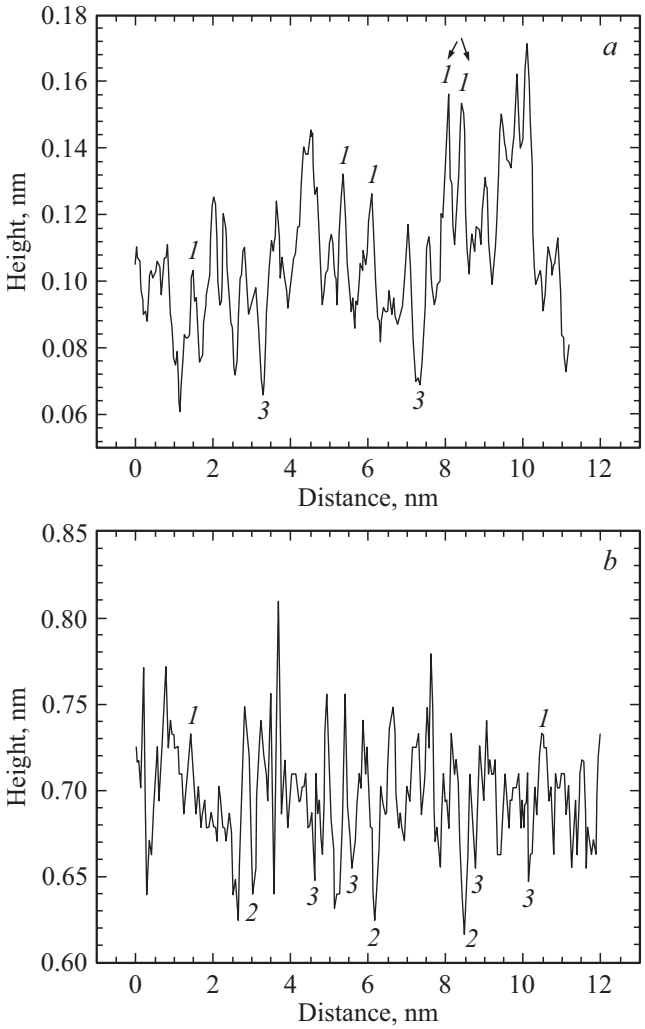

Figure 3. Local (0001) surface profiles of the p-$Bi_{0.5}Sb_{1.5}Te_3$ TI films in different regions of surface morphology images (a, b). *1* — Antisite Bi_{Te} defects; closely spaced Bi_{Te} defects are indicated in panel *a*. *2* — Te (V_{Te}) vacancy. *3* — impurity $Sb \rightarrow Bi$ substitution defects.

decreases. Optimization of the film fabrication technology affects the formation of defects and provides an opportunity to compensate the reduction in electrical conductivity, which ensures an enhancement of thermoelectric efficiency to $Z_{max} = 4.35 \cdot 10^{-3}\,K^{-1}$ at $T = 240\,K$ in the p-$Bi_{0.5}Sb_{1.5}Te_3$ films [14].

3. STS spectra

STS studies were performed by measuring differential tunneling conductance dI_t/dU as function of voltage U in arbitrary (0001) surface regions of the p-Bi_2Te_3 and p-$Bi_{0.5}Sb_{1.5}Te_3$ films. These measurements were carried out with feedback disabled, a frequency of 7 kHz, and a modulation voltage of 5−10 mV at a fixed height of the tungsten probe above the surface and a resolution of 1.5 mV [24].

The position of the Dirac point relative to the Fermi level, the Dirac point energy fluctuations, the edges of the valence band (E_V) and the conduction band (E_C), and energy gap E_g were determined by analyzing the normalized dependences of dI_t/dU on U (Figure 4).

The shape of dependences of dI_t/dU on U, especially those in the p-$Bi_{0.5}Sb_{1.5}Te_3$ films (Figure 4, *b*), may be attributed to fluctuations in the density of states due to the high density of defects (especially V_{Te} vacancies; see Figures 1, *b*; 3, *b*). As illustrated in Figure 4, Dirac point E_D in the studied films is located in the valence band [11,25], and energy E_D has fluctuations ΔE_D that are determined relative to the average value: $\Delta E_D/\langle E_D\rangle$. In the p-$Bi_{0.5}Sb_{1.5}Te_3$ films, $\Delta E_D/\langle E_D\rangle$ fluctuations in different surface fragments varied from 2 to 16%. The E_D fluctuation interval in the p-Bi_2Te_3 films was 10−18%.

The position of the edges of valence (E_V) and conduction (E_C) bands in the studied films was determined by the method of normalized differential conductance from the inflection points of dependence $(dI_t/dU)/(|I_t|(U))$ [26]. Point $I = 0$, $U = 0$ was excluded when the E_V and E_C band edges were determined. To obtain more accurate positions of E_V and E_C, d^2I_t/dU^2 was calculated additionally [10]. In addition to ΔE_D fluctuations, the investigated films also feature E_V and E_C energy fluctuations. The average $\Delta E_V/\langle E_V\rangle$ and $\Delta E_C/\langle E_C\rangle$ values in different fragments of the surface of p-$Bi_{0.5}Sb_{1.5}Te_3$ films (Figure 4) were close and varied from 5 to 20%. Energy gap E_g determined with account for fluctuations of E_V and E_C differs by no more than 1% from the average value (Figure 4) both in the p-$Bi_{0.5}Sb_{1.5}Te_3$ films ($\langle E_g\rangle = 238$ meV) and in the p-Bi_2Te_3 films ($\langle E_g\rangle = 198$ meV). Owing to band inversion in TIs [3–5], the values of E_g in films determined by the STS method are higher than those derived from optical data ($E_g = 200$ meV [6,23] in p-$Bi_{0.5}Sb_{1.5}Te_3$ and $E_g = 150$ meV [24,27] in p-Bi_2Te_3). When the spectra of optical absorption in films are studied, effective energy gap E_g is measured, which corresponds to the average distance between the edges of bands E_V and E_C. Owing to band inversion, this distance is shorter than the maximum one between the E_V and E_C edges in TIs.

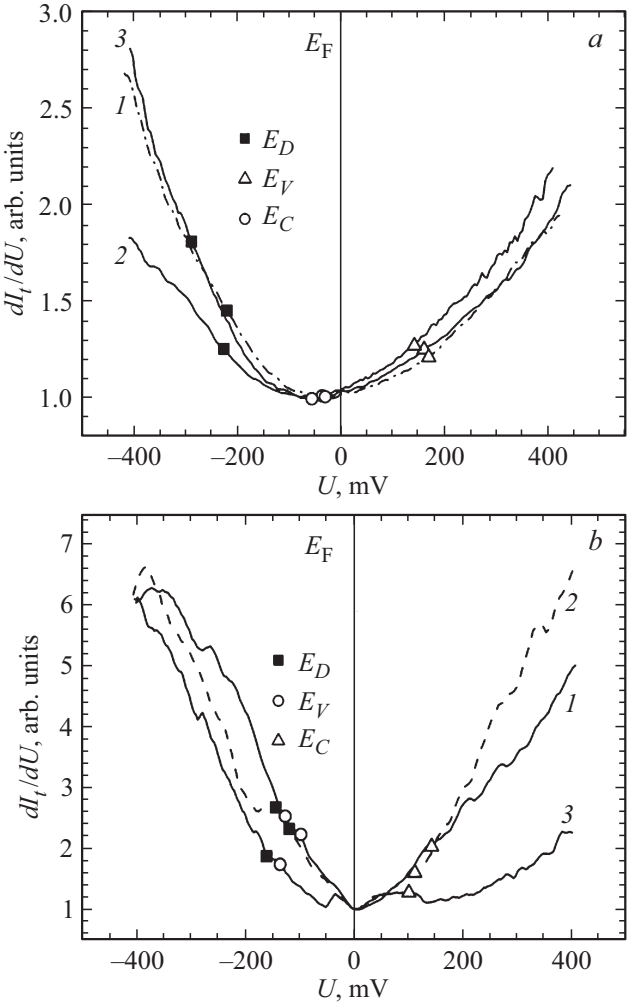

Figure 4. Differential tunneling conductance dI_t/dU as function of voltage U in different fragments *1*−*3* of the surface of (*a*) p-Bi_2Te_3 and (*b*) p-$Bi_{0.5}Sb_{1.5}Te_3$ films.
(*a*) p-Bi_2Te_3, Dirac point energy E_D, meV: *1* — (−220), *2* — (−226), *3* — (−288), valence band edge energy E_V, meV: *1* — (−31), *2* — (−36), *3* — (−56), conduction band edge energy E_C: *1* — 169, *2* — 161, *3* — 142.
(*b*) p-$Bi_{0.5}Sb_{1.5}Te_3$ E_D: *1* — (−118), *2* — (−143), *3* — (−160); valence band edge energy E_V, meV: *1* — (−97), *2* — (−126), *3* — (−135), conduction band edge energy E_C, meV: *1* — 143, *2* — 112, *3* — 101.

The detected E_D, E_V, and E_C energy fluctuations in the p-$Bi_{0.5}Sb_{1.5}Te_3$ and p-Bi_2Te_3 films are governed by fluctuations of the density of states on the TI surface and are consistent with the changes in H_M and H_S that characterize height distortions in the distribution of Te(1) atoms on the (0001) surface.

In p-type materials, Dirac point energy E_D was determined as the point of intersection between the line representing the extrapolation of the linear dispersion section of fermions (dI_t/dU) and the energy dependence

coordinate (U) [11,25]. This method of E_D determination is based on the fact that when band edges are inverted, the valence band edge is distorted significantly greater by electron filling than the conduction band edge.

According to STS [11,25] and ARPES [6,11] spectra, the Dirac point in the p-Bi_2Te_3 films is located in the valence band (Figure 4, a). The position of Dirac point E_D (Figure 4, a) in the p-Bi_2Te_3 films with a thickness of approximately $2\,\mu$m formed by discrete evaporation is consistent with the results of examination of ARPES spectra of thin p-Bi_2Te_3 films with $t = 6$ nm produced by MBE [6].

In the p-$Bi_{0.5}Sb_{1.5}Te_3$ solid solution films (Figure 4, b), Dirac point E_D (Figure 4, b) shifts to the energy gap, remaining near the valence band edge; the average $\langle E_D \rangle$ value is -21 meV relative to E_V. According to ARPES data [6], E_D in the p-$Bi_{0.5}Sb_{1.5}Te_3$ films at $t = 6$ nm is located in a deep „saddle“ formed in the energy gap as a result of distortion of the valence band edges associated with band inversion in TIs. The Dirac point in the p-$Bi_{0.5}Sb_{1.5}Te_3$ film thus shifts into the energy gap, and $E_D = 75$ meV relative to E_V.

Although the thicknesses of films differed significantly, fairly close E_D values were obtained by analyzing the Dirac point position (E_D) relative to Fermi level E_F in both STS and ARPES data for the p-Bi_2Te_3 and p-$Bi_{0.5}Sb_{1.5}Te_3$ films. In the p-Bi_2Te_3 films, the average $\langle E_D \rangle$ values derived from the STS spectra with account for fluctuations of the Dirac point are -245 MeV (Figure 4, a), while ARPES data yield $E_D = -270$ MeV [6]. In the p-$Bi_{0.5}Sb_{1.5}Te_3$ films, $\langle E_D \rangle = -140$ meV (Figure 4, b) and $E_D = -170$ meV [6] according to STS and ARPES data, respectively.

Fermi level E_F in the p-Bi_2Te_3 and p-$Bi_{0.5}Sb_{1.5}Te_3$ films is located in the energy gap above the Dirac point (Figure 4). Although the films have p-type bulk conductivity, electrons are found on the surface of films with this mutual positioning of E_D and E_F (owing to band inversion in TIs), which is verified by the presence of tellurium vacancies V_{Te} that enable the emergence of surface electrons. A similar conclusion regarding the presence of electrons on the surface of films of the same composition with Fermi level E_F positioned above Dirac point E_D was made by analyzing ARPES data [6]; notably, the Hall resistance of films measured as a function of the magnetic field was negative. Holes appear on the surface of films of p-$Bi_{2-x}Sb_xTe_3$ solid solutions in compositions with $x \geq 1.76$ when Fermi level E_F is positioned below Dirac point E_D [6].

The presence of tellurium vacancies V_{Te} in the p-Bi_2Te_3 and p-$Bi_{0.5}Sb_{1.5}Te_3$ films (Figures 2, 3), which are associated with surface electrons in TI films, suggests that V_{Te} vacancies are instrumental to shaping the (0001) surface relief and altering the average $\langle H_M \rangle$ and root-mean-square $\langle H_S \rangle$ height deviations of distortions in the distribution of Te(1) atoms on the surface.

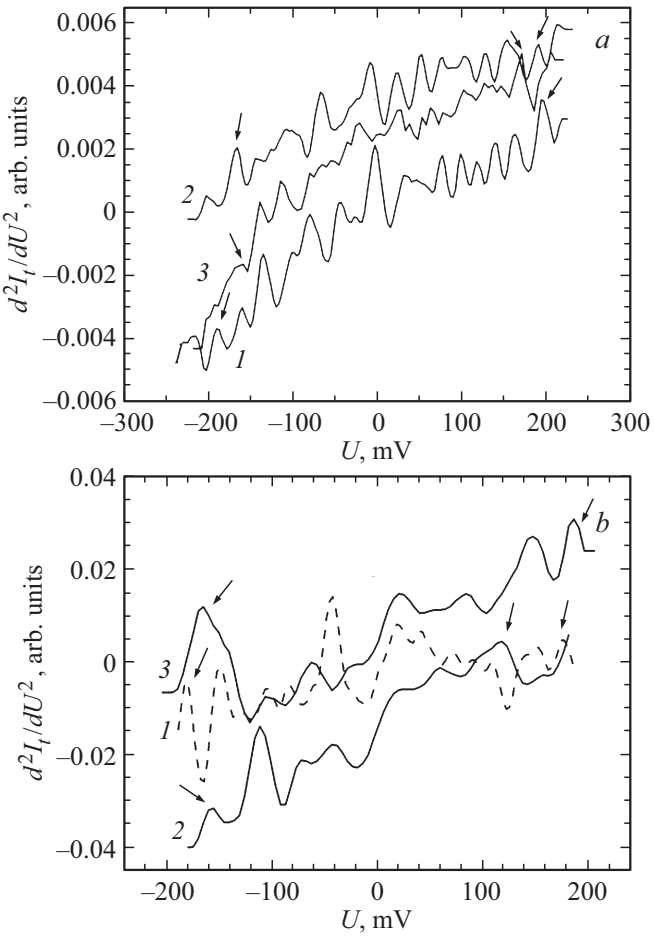

Figure 5. Derivatives of differential tunneling conductance dI_t/dU as functions of voltage U in (a) p-Bi_2Te_3 and (b) p-$Bi_{0.5}Sb_{1.5}Te_3$ films. The intervals of variation of defect level energy E_p are indicated by arrows.

4. Energies of defect levels

Surface levels formed by defects in the p-$Bi_{0.5}Sb_{1.5}Te_3$ and p-Bi_2Te_3 films are observed as p_i peaks in the normalized dependences of dI_t/dU on U after additional differentiation (Figure 5).

In the p-$Bi_{0.5}Sb_{1.5}Te_3$ film, the E_p energies of defect levels defined relative to the Dirac point as $E_p(E_D) = E_p - E_D$ are (7.5–305) meV, (–40–235) meV and (–22–293) meV for different surface fragments. In the p-Bi_2Te_3 film, the values of $E_p(E_D)$ are (32–414) meV, (25–415) meV, and (130–460) meV (Figure 5, b); i. e., the energies of defect levels detected in the p-Bi_2Te_3 film were higher than those corresponding to the p-$Bi_{0.5}Sb_{1.5}Te_3$ solid solution with low thermal conductivity and high thermoelectric efficiency [14].

The influence of surface states of Dirac fermions in layered Bi_2Te_3-based TI films on their thermoelectric properties was studied in [28]. According to [28], the contribution of surface states to electrical conductivity in micrometer-thick films is 10% at room temperature and up to 80% at low temperatures. The effect of Dirac

fermions on Seebeck coefficient S, electrical conductivity σ, and the power factor measured at the (0001) interlayer surface as functions of pressure P at room temperature in the p-$Bi_{0.5}Sb_{1.5}Te_3$ films with a thickness of $2-3\,\mu$m was examined in [29]. Electronic isostructural topological phase transitions associated with surface states of Dirac fermions [29] were observed in the $S(P)$ dependences at pressures under which the power parameter was maximized.

The effect of Dirac surface fermions on the thermoelectric properties of the p-Bi_2Te_3 and p-$Bi_{0.5}Sb_{1.5}Te_3$ films was determined based on surface concentration n_s and Fermi velocity v_F in the form of $n_s = k^2F/4\pi$, where wave vector $k_F = |E_D|/\hbar \cdot v_F$. The values of $v_F = 3.3 \cdot 10^5\,\mathrm{ms}^{-1}$ and $v_F = 3.8 \cdot 10^5\,\mathrm{ms}^{-1}$ were used for p-Bi_2Te_3 and p-$Bi_{0.5}Sb_{1.5}Te_3$, respectively [6]. Fluctuations of Dirac point energy E_D were taken into account in calculations of n_s (Figure 4).

Estimates of surface concentration n_s of fermions revealed that it reaches $n_s = (8.15-13.8) \cdot 10^{12}\,\mathrm{cm}^{-2}$ and $n_s = (1.75-3.25) \cdot 10^{12}\,\mathrm{cm}^{-2}$ with account for E_D fluctuations in the p-Bi_2Te_3 and p-$Bi_{0.5}Sb_{1.5}Te_3$ films, respectively. The average values of n_s are $1 \cdot 10^{13}\,\mathrm{cm}^{-2}$ and $2.5 \cdot 10^{12}\,\mathrm{cm}^{-2}$ in the p-Bi_2Te_3 and p-$Bi_{0.5}Sb_{1.5}Te_3$ films, respectively. In p-$Bi_{0.5}Sb_{1.5}Te_3$, the reduction in n_s is accompanied by lowering of Dirac point energy $|E_D|$ and its shift to the top of the valence band, while Fermi velocity v_F increases compared to the one in p-Bi_2Te_3. At the same time, the density of surface defects in the p-$Bi_{0.5}Sb_{1.5}Te_3$ films is higher than in the p-Bi_2Te_3 films. The higher surface concentration n_s value in p-Bi_2Te_3 defines the contribution of surface Dirac fermions to the thermoelectric properties, while the increase in fermion velocity in p-$Bi_{0.5}Sb_{1.5}Te_3$ translates into an increased surface conductivity via an enhanced contribution of surface mobility [28,30].

5. Conclusion

STM studies of the (0001) interlayer surface morphology in layered TI films of p-Bi_2Te_3 and solid solution p-$Bi_{0.5}Sb_{1.5}Te_3$ revealed that the intensity fluctuations in morphology images are associated with the formation of intrinsic acceptor antisite Bi_{Te} defects and tellurium vacancies V_{Te}, which emerge in the process of film growth by discrete evaporation. Impurity $Sb \rightarrow Bi$ substitution defects are also produced in the p-$Bi_{0.5}Sb_{1.5}Te_3$ films in the process of formation of a solid solution. Vacancy density V_{Te} and average $\langle H_M \rangle$ and root-mean-square $\langle H_S \rangle$ height deviations in the distribution of Te(1) atoms on the (0001) surface in a solid solution in p-$Bi_{0.5}Sb_{1.5}Te_3$ were higher than those in p-Bi_2Te_3.

A higher density of defects in the p-$Bi_{0.5}Sb_{1.5}Te_3$ films leads to a reduction in thermal conductivity; however, the electrical conductivity also decreases. Optimization of the film fabrication technology affects the formation of defects and provides an opportunity to compensate the reduction in electrical conductivity, which ensures an enhancement of thermoelectric efficiency in the p-$Bi_{0.5}Sb_{1.5}Te_3$ films produced by discrete evaporation.

The analysis of normalized dependences of tunneling conductance dI_t/dU on voltage U measured by scanning tunneling spectroscopy revealed that Dirac point E_D determined relative to the Fermi energy is located in the valence band in the examined films, and energy E_D in the p-$Bi_{0.5}Sb_{1.5}Te_3$ films is shifted noticeably to the top of the valence band (compared to p-Bi_2Te_3).

It was found that Fermi level E_F in the p-Bi_2Te_3 and p-$Bi_{0.5}Sb_{1.5}Te_3$ films is positioned above the Dirac point. Therefore, owing to band inversion in TIs, electrons are found on the surface of films, which is verified by the presence of tellurium vacancies V_{Te}; the films themselves have p-type bulk conductivity.

Fluctuations of the Dirac point energy $(\Delta E_D/\langle E_D \rangle)$, the valence band edge $(\Delta E_V/\langle E_V \rangle)$, and the energies of surface defect levels (E_p) associated with variations of the density of states on the (0001) surface in the p-$Bi_{0.5}Sb_{1.5}Te_3$ were less pronounced than those in p-Bi_2Te_3.

It follows from the estimates of surface concentration n_s of Dirac fermions that the contribution of surface fermions to the thermoelectric properties is governed by the growth of n_s to $1 \cdot 10^{13}\,\mathrm{cm}^{-2}$ in the p-Bi_2Te_3 films and by an increase in velocity of Dirac fermions and, consequently, surface mobility in the p-$Bi_{0.5}Sb_{1.5}Te_3$ films.

Conflict of interest

The authors declare that they have no conflict of interest.

References

[1] Modules, Systems, and Applications in Thermoelectrics / Ed. D.M. Rowe. CRC Press, Boca Raton (2012).
[2] M.J. Gilbert. Commun. Phys. **4**, *1*, 70 (2021).
[3] J. Heremans, R. Cava, N. Samarth. Nature Rev. Mater. **2**, *10*, 17049 (2017).
[4] M.Z. Hasan, C.L. Kane. Rev. Mod. Phys. **82**, *4*, 3045 (2010).
[5] Y.L. Chen, J.G. Analytis, J.H. Chu, Z.K. Liu, S.K. Mo, X.L. Qi, H.J. Zhang, H. Lu, X. Dai, Z. Fang, S.C. Zhang, I.R. Fisher, Z. Hussain, Z.X. Shen. Science. **325**, *5937*, 178 (2009).
[6] J. Zhang, C.-Z. Chang, Z. Zhang, J. Wen, X. Feng, K. Li, M. Liu, K. He, L. Wang, X. Chen, Q.-K. Xue, X. Ma, Y. Wang. Nature Commun. **2**, *1*, 574 (2011).
[7] T. Knispel, W. Jolie, N. Borgwardt, J. Lux, Z. Wang, Y. Ando, A. Rosch, T. Michely, M. Gruninger. Phys. Rev. B **96**, *19*, 195135 (2017).
[8] A.A. Taskin, Z. Ren, S. Sasaki, K. Segawa, Y. Ando. Phys. Rev. Lett. **107**, *1*, 016801 (2011).
[9] Y. Ando. J. Phys. Soc. Jpn. **82**, *10*, 102001 (2013).
[10] H. Nam, Y. Xu, I. Miotkowski, J. Tian, Y.P. Chen, C. Liu, C.K. Shih. J. Phys. Chem. Solids **128**, 251 (2019).
[11] Z. Alpichshev, J.G. Analytis, J.-H. Chu, I.R. Fisher, Y.L. Chen, Z.X. Shen, A. Fang, A. Kapitulnik. Phys. Rev. Lett. **104**, *1*, 016401 (2010).
[12] X. He, H. Li, L. Chen, K. Wu. Sci. Rep. **5**, *1*, 8830 (2015).
[13] R. Rejali, L. Farinacci, S. Otte. Phys. Rev. B **107**, *3*, 035406 (2023).

[14] L.N. Lukyanova, Y.A. Boikov, O.A. Usov, V.A. Danilov, I.V. Makarenko, V.N. Petrov. Magnetochemistry **9**, *6*, 141 (2023).
[15] D.L. Medlin, Q.M. Ramasse, C.D. Spataru, N.Y.C. Yang. J. Appl. Phys. **2010**, *108*, 4, 043517.
[16] H. Beidenkopf, P. Roushan, J. Seo, L. Gorman, I. Drozdov, Y.S. Hor, R.J. Cava, A. Yazdani. Nature Phys. **7**, *12*, 939 (2011).
[17] X. Chen, H.D. Zhou, A. Kiswandhi, I. Miotkowskii, Y.P. Chen, P.A. Sharma, A.L. Lima Sharma, M.A. Hekmaty, D. Smirnov, Z. Jiang. Appl. Phys. Let. **99**, *26*, 261912 (2011).
[18] P. Dutta, D. Bhoi, A. Midya, N. Khan, P. Mandal, S. Shanmukharao Samatham, V. Ganesan. Appl. Phys. Lett. **100**, *25*, 251912 (2012).
[19] W. Ko, I. Jeon, H.W. Kim, H. Kwon, S.-J. Kahng, J. Park, J.S. Kim, S.W. Hwang, H. Suh. Sci. Rep. **3**, *1*, 2656 (2013).
[20] S. Jia, H. Beidenkopf, I. Drozdov, M.K. Fuccillo, J. Seo, J. Xiong, N.P. Ong, A. Yazdani. Phys. Rev. B **86**, *16*, 165119 (2012).
[21] T. Zhu, L. Hu, X. Zhao, J. He. Adv. Sci. **3**, *7*, 1600004 (2016).
[22] J.C. Slater. J. Chem. Phys. **41**, *10*, 3199 (1964).
[23] D. Bessas, I. Sergueev, H.-C. Wille, J. Person, D. Ebling, R.P. Hermann. Phys. Rev. B **86**, *22*, 224301 (2012).
[24] L.N. Lukyanova, I.V. Makarenko, O.A. Usov, P.A. Dementev. Semicond. Sci. Technol., **33**, *5*, 055001 (2018).
[25] M. Chen, J. Peng, H. Zhang, L. Wang, K. He, X. Ma, Q. Xue. Appl. Phys. Lett. **101**, *8*, 081603 (2012).
[26] C. Wagner, R. Franke, T. Fritz. Phys. Rev. B **75**, *23*, 235432 (2007).
[27] J.G. Austin, A. Sheard. J. Electron. Control **3**, *2*, 236 (1957).
[28] S.Y. Matsushita, K. Ichimura, K.K. Huynh, K. Tanigaki. Phys. Rev. Mater. **5**, *1*, 014205 (2021).
[29] I.V. Korobeinikov, N.V. Morozova, L.N. Lukyanova, O.A. Usov, S.V. Ovsyannikov. Semiconductors **53**, *6*, 732 (2019).
[30] Y. Xu, I. Miotkowski, C. Liu, J. Tian, H. Nam, N. Alidoust, J. Hu, C.-K. Shih, M.Z. Hasan, Y.P. Chen. Nat. Phys. **10**, *12*, 956 (2014).

Translated by D.Safin